A TEXTURE COMPONENT CRYSTAL PLASTICITY FINITE ELEMENT METHOD FOR SCALABLE ANISOTROPY SIMULATIONS

MAX-PLANCK PROJECT REPORT

D. Raabe[1], K. Helming[2], F. Roters[1], J. Hirsch[3]

[1] Max-Planck-Institut für Eisenforschung, Abteilung für Mikrostrukturphysik und Umformtechnik, Max-Planck-Str. 1, 40237 Düsseldorf, Germany

[2] Physikalisches Institut, TU Clausthal, Leibnizstrasse 4, 38678 Clausthal-Zellerfeld, Germany

[3] Hydro, P.O. Box 2468, 53014 Bonn, Germany

*http://*www.mpg.de *http://*www.mpie.de *http://edoc.mpg.de/*

Keywords: texture, crystal plasticity, finite element simulation, polycrystal, anisotropy, metal forming, texture change, yield surface, single crystal, slip systems, micromechanics, aluminium

Report Abstract

This progress report introduces a crystal plasticity finite element method which includes and updates the texture of polycrystalline matter for physically based simulations of large strain forming operations. The approach works by directly mapping a set of discrete texture components into a crystal plasticity finite element method. The method is well suited for industrial applications since it is formulated on the basis of existing commercial software solutions. The study gives an overview of the new texture component crystal plasticity finite element method and presents examples.

The Basic Problem of Constitutive Anisotropy Modeling

Engineering metals subject to forming operations typically have crystallographic textures which they inherit from proceeding processing steps. The intrinsic elastic and plastic anisotropy of crystalline matter entails an overall anisotropic response of such specimens when mechanically loaded. This behavior imposes two basic problems. The first challenge is the formulation of methods to map the *initial* anisotropy into classical mathematical approaches for predicting large strain deformation. The second even more demanding goal is the description of the *change* of crystalline anisotropy during forming. This is necessary since the crystals rotate during deformation owing to the antisymmetry of the crystalline displacement gradients. The first problem can be solved using adequate yield surface functions. The second problem cannot be solved by a statistical constitutive law since each crystal takes an individual re-orientation path during forming. Translating this into the yield surface concept means that any constitutive evolution law for the shape function of the yield surface depends on at least 10^3 possible discrete texture components with potentially individual behavior as well as on the imposed stress and strain rate states. Rendering this into a simple constitutive form is practically hopeless. For this purpose we have developed a new efficient and at the same time physically rooted prediction method for the simulation of polycrystal plasticity which accounts for these two crystallographic aspects [1,2]. It is based on directly mapping discrete orientation components onto the integration points of a crystal plasticity finite element model. The texture components can be extracted from experimental data, such as pole figures stemming from x-ray or electron diffraction.

Introduction to Using Texture Components in a Crystal Plasticity FE Constitutive Model

As outlined above the main issue of large-strain large-specimen crystal plasticity metal forming simulations is to tackle both, the anisotropy due to the starting texture and due to texture evolution. One method could be to simply assign each grain orientation to a separate integration point. However, such a brute force approach is not feasible when aiming at the simulation of larger parts containing $\sim 10^{10}$ grains (e.g. automotive parts made of 6xxx aluminium or IF steel). This essential limitation suggests the employment of a more compact mathematical form to map and update textures of large parts properly during metal forming simulations. Crystal plasticity finite element approaches which update the texture require a *discrete* representation of the orientation distribution function or a portion of it at each integration point. Mapping such a discrete portion of the global texture requires the reduction of the information content to a level at which complex deformation processes can be simulated at reasonable computation costs. Such a form is offered by the texture

component method. It approximates the orientation distribution function by a superposition of sets of simple standard functions with individual coordinates, orientation density, and scatter in orientation space. Such a representation of a preferred orientation is referred to as a texture component. In contrast to the use of global symmetric Wigner functions for instance in the Fourier-type series expansion methods [3], the texture component method is based on using spherical normalized localized standard functions [4-6]. The superposition can be expressed by

$$f(g) = F + \sum_{c=1}^{C} I^c f^c(g) = \sum_{c=0}^{C} I^c f^c(g) \quad \text{where} \quad I^0 = F,\ f^0(g) = 1 \tag{1}$$

where g is the orientation, $f(g)$ is the orientation distribution function, F is the volume portion of all randomly oriented crystals (random texture component), I^c is the volume portion of all crystals which belong to the texture component c (Fig. 1). The orientation distribution function is defined by

$$f(g)\,\mathrm{d}g = 8\pi^2 \frac{\mathrm{d}V_g}{V} \qquad \text{which implies} \qquad f(g) \geq 0 \tag{2}$$

where V is the sample volume and $\mathrm{d}V_g$ the volume of all crystals with an orientation g within the orientation portion $\mathrm{d}g = \sin(\phi)\,\mathrm{d}\phi\,\mathrm{d}\varphi_1\,\mathrm{d}\varphi_2$. Normalization requires

$$\oint f^c(g)\,\mathrm{d}g = 1 \qquad \text{which implies} \qquad \sum_{c=0}^{C} I^c = 1 \tag{3}$$

As a rule texture components require positivity, i.e.

$$f^c(g) \geq 0 \quad \text{for all} \quad g \in G \qquad \text{and} \qquad I^c > 0 \tag{4}$$

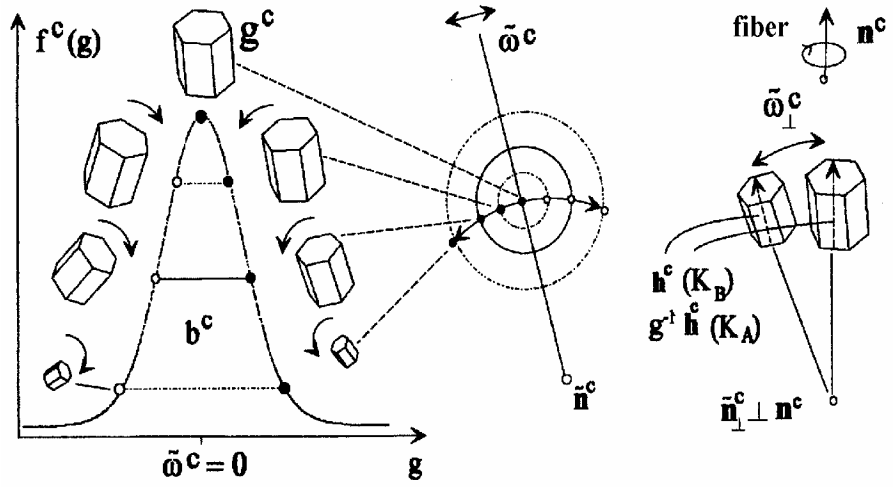

Fig 1 Schematical sketch of a spherical texture component c with a preferred orientation g^c and scatter width b^c. $f^c(g)$ only depends on $\tilde{\omega}^c = \tilde{\omega}(g^c, g)$, i.e. it is independent on the rotation axis $\tilde{n}^c$ [5,6].

where G is the orientation space. Eq. 4 can also be derived by using Eq. 2 and the assumption that the texture components do not overlap in orientation space and that an orientation distribution function can be described by one single texture component. Distribution functions which have a maximum at a preferred orientation g^c and decrease with increasing orientation distance $\tilde{\omega}^c = \tilde{\omega}(g^c, g)$ are referred to as central functions. Such functions, including corresponding pole figures, can be generally represented in the form of series expansions of χ functions or respectively Legendre polynomials. More practical approximations of texture component have been introduced on the basis of spherical Gauß- and Lorentz-functions. Although these functions are not exactly in accord with the central limit theorem they can be represented in an analytically closed form (Table 1). For the examples presented in this report we used Gauß functions to decompose the texture. The texture component method provides a small set of compact functions which are characterized by simple parameters of physical significance (Euler angles, scatter, volume fraction). Usually, only a few texture components are required for representing

textures in a precise mathematical form. The inherent data reduction drastically enhances the computational efficiency of the subsequent finite element simulation (Fig. 2).
Aluminium textures can be reproduced by using small sets of discrete texture components together with a random background component. The most important of these components in aluminium and other face centered cubic metals are the Cube-component ({001}<100>, φ_1=0°, ϕ=0°, φ_2=0°), the Goss-component ({011}<100>, φ_1=0°, ϕ=45°, φ_2=0°), the Brass–component ({0$\underline{1}$1}<211>, φ_1=35°, ϕ=45°, φ_2=0°), the Copper–component ({$\underline{2}$11}<111>, φ_1=90°, ϕ=35°, φ_2=45°), and the S–component (~{12$\underline{3}$}<634>, φ_1=60°, ϕ=32°, φ_2=65°).

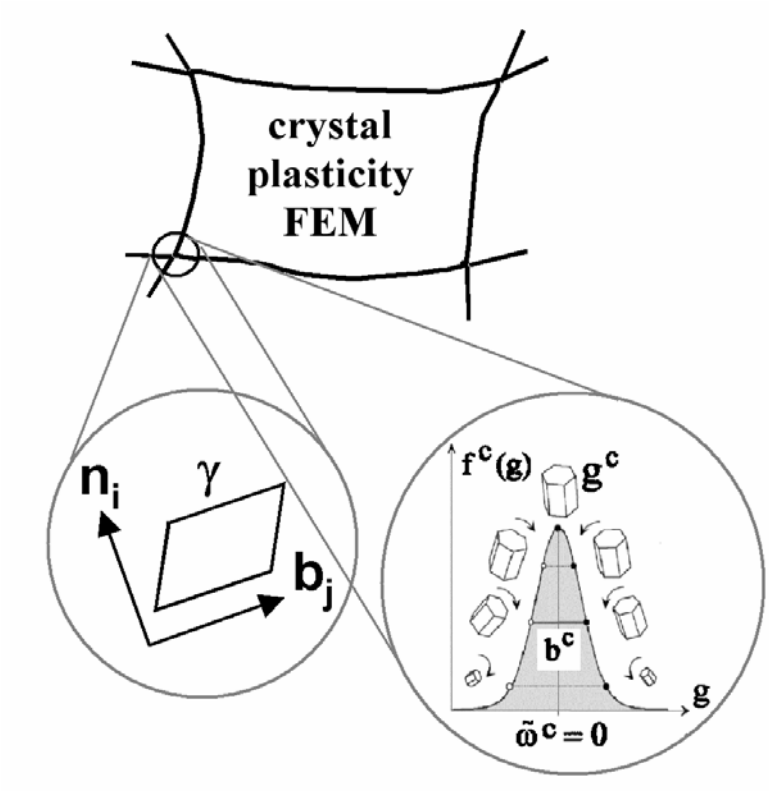

Fig 2 Basic set-up of the texture component crystal plasticity finite element method [5,6].

The texture components are extracted from experimentally obtained pole figures (x-ray diffraction, neutron diffraction) or single orientation data sets (electron diffraction) by identifying the main texture maxima and the suggested scatter width and by minimizing the deviation between the original (experimental) texture and the one created by the texture component functions in an iterative fashion. Depending on the experience in interpreting crystallographic textures the user can specify the position, height, and scatter of the texture components within certain bounds during the minimization. This makes sense, when the number of texture components initially prescribed to match an experimental texture is small or when a certain scatter width of the components should not be exceeded. Subsequently, the so extracted texture components must be mapped onto the integration points of a finite element mesh. This is conducted in two steps. First, the discrete center orientation (mean orientation, preferred orientation) of each texture component is assigned in terms of its respective Euler triple (φ_1, ϕ, φ_2) onto each of the integration points. It is important in this context, that the use of the Taylor assumption locally allows us to map more than one crystallographic orientation on each integration point. Second, all center orientations of the components that were initially assigned to the integration points are now rotated in a fashion that the resulting distribution of all these new orientations deviating from the initial center orientation reproduces exactly the desired texture function extracted from experiment. In other words the orientation scatter individually described by each texture component function is mapped onto the finite element by systematically modifying the orientations at each point in a way which exactly imitates the scatter prescribed by the texture component. This means that the scatter which was originally only given in orientation space is now matched by an equivalent scatter both, in real space and in orientation space.

Standard Distributions				
type	**Gauß**		**Lorentz**	
form	**sphere**	**fiber**	**sphere**	**fiber**
ODF f(g)	$N\, e^{S\cos\tilde{\omega}}$ $N = \left[I_0(S) - I_1(S)\right]^{-1}$	$N_\perp \exp\left(S_\perp \cos\tilde{\omega}_\perp\right),$ $N_\perp = S_\perp / \sinh S_\perp$	$\dfrac{(1+T)^2 + 4T\cos^2\dfrac{\tilde{\omega}}{2}}{\left[(1+T)^2 - 4T\cos^2\dfrac{\tilde{\omega}}{2}\right]^2} \times (1-T)$	$\dfrac{1-T_\perp^2}{\left(1-2T_\perp\cos\tilde{\omega}_\perp + T_\perp^2\right)^{3/2}}$
scatter parameter	$S = \dfrac{\ln 2}{1-\cos(b/2)}$	$S_\perp = \dfrac{\ln 2}{1-\cos(b_\perp/2)}$	$T = \left(\sqrt{\tau} - \sqrt{\tau - 1}\right)^2$ *	$T_\perp = R - \sqrt{R^2 - 1},$ $R = \dfrac{2^{2/3} - \cos(b_\perp/2)}{2^{2/3} - 1}$
coefficients C_l	$N\left[I_l(S) - I_{l+1}(S)\right]$	$(2l+1)\sqrt{\dfrac{\pi}{2S_\perp}}\, I_{l+1/2}(S_\perp)$	$(2l+1)\, T^l$	$(2l+1)\, T_\perp^l$
pole figure	$N \exp\left(S\sin(\tilde{\vartheta}/2)\right)$ $\times I_0\left(S\cos(\tilde{\vartheta}/2)\right)$	$N_\perp \exp\left(S_\perp \cos\vartheta_h \cos\vartheta_y\right)$ $\times I_0\left(S_\perp \sin\vartheta_h \sin\vartheta_y\right)$ $\vartheta_h = \sphericalangle(\mathbf{h}^c, \mathbf{h}),$ $\vartheta_y = \sphericalangle(\mathbf{y}^c, \mathbf{y})$	$\dfrac{1-T^2}{\left(1-2T\cos\tilde{\vartheta} + T^2\right)^{3/2}}$	$\dfrac{2\left(1-T_\perp^2\right)}{\pi(C-D)\sqrt{C+D}}$ $\times E\left(\dfrac{2D}{C+D}\right)$ **

* $\tau = \dfrac{2}{3}\left(19c^2 - 34c + 19\right)^{1/2} \cos\left\{\dfrac{1}{3}\arccos\left[\dfrac{-82c^3 + 240c^2 - 246c + 80}{\left(19c^2 - 34c + 19\right)^{3/2}}\right]\right\} + \dfrac{5-4c}{3}; \quad c = \cos^2\dfrac{b}{4}$

** $C = 1 + T_\perp^2 - 2T_\perp \cos\vartheta_h \cos\vartheta_y, \quad D = 2T_\perp \sin\vartheta_h \sin\vartheta_y, \quad E(x) = \int_0^{\pi/2} (1 - x\sin^2\varphi)\, d\varphi$

Table 1 Various types of standard texture component distributions including series coefficients and pole figures. $I_0(x)$ and $I_1(x)$ are generalized Bessel functions [6].

Constitutive Model for the Crystal Plasticity Finite Element Simulations

In the large-strain constitutive crystal plasticity model [7] modified for the present study [1,2] one assumes the stress response at each macroscopic continuum material point to be potentially given by one crystal or by a volume-averaged response of a set of grains comprising the respective material point. The latter assumption can be referred to as a local Taylor-type or local strain-rate homogenization assumption. In case of a multi-grain description the volume averaged stress amounts to

$$\langle \mathbf{T} \rangle = \sum_{k=1}^{N} \left(w_k \mathbf{T}_k \right) \tag{5}$$

where N is the total number of individual orientations mapped onto an integration point using the Taylor assumption, w_k the volume fraction of each single orientation extracted from a texture

component as described above, $\mathbf{T}_k$ the Cauchy stress produced by the *kth* individual orientation, and <**T**> the volume average stress produced by all orientation mapped at the integration point. The constitutive equation for the stress in each grain is then expressed in terms of

$$\mathbf{T^*} = \mathbf{C}\mathbf{E^*} \tag{6}$$

where **C** is the fourth order elastic tensor and **E*** an elastic strain measure obtained by polar decomposition,

$$\mathbf{E^*} = \frac{1}{2}\left(\mathbf{F^{*T}}\,\mathbf{F^*}\,\mathbf{-1}\right) \tag{7}$$

which leads to a stress measure which is the elastic work conjugate to the strain measure **E***,

$$\mathbf{T^*} = \mathbf{F^{*-1}}\left(\det\left(\mathbf{F^*}\right)\mathbf{T}\right)\mathbf{F^{*-T}} \tag{8}$$

where **T** is the symmetric Cauchy stress tensor in the grain, and **F*** is a local elastic deformation gradient defined in terms of the local *total* deformation gradient **F** and the local *plastic* deformation gradient $\mathbf{F}^{\mathrm{p}}$. The relation between the elastic and the plastic portion of **F** amounts to

$$\mathbf{F^*} = \mathbf{F}\mathbf{F}^{\mathrm{p}^{-1}}, \quad \det(\mathbf{F^*}) > 0, \quad \det(\mathbf{F}^{\mathrm{p}}) = 1 \tag{9}$$

The plastic deformation gradient is given by the flow rule

$$\dot{\mathbf{F}}^{\mathrm{p}} = \mathbf{L}^{\mathrm{p}}\,\mathbf{F}^{\mathrm{p}} \tag{10}$$

with its crystalline portion

$$\mathbf{L}^{\mathrm{p}} = \sum_{k=1}^{N} \dot{\gamma}_k\, \mathrm{m}_k, \qquad \mathrm{m}_k = \hat{\mathrm{b}}_k \otimes \hat{\mathrm{n}}_k \tag{11}$$

where m_k are the *k*th dyadic slip products of unit vectors $\hat{\mathrm{b}}_k$ in the slip direction and $\hat{\mathrm{n}}_k$ normal to the slip plane, and $\dot{\gamma}_k$ the shear rates on these systems. The specific constitutive functions for the plastic shearing rates $\dot{\gamma}_k$ on the slip systems are taken as

$$\dot{\gamma}_k = \dot{\gamma}_0 \left| \frac{\tau_k}{\tau_{k,crit}} \right|^{1/m} \mathrm{sign}(\tau_k) \tag{12}$$

where τ_k is the resolved shear stress for the slip system *k*, and $\tau_{k,\,\mathrm{crit}}$ is the actual critical shear stress on the *k*th slip system. $\dot{\gamma}_0$ and *m* are material parameters representing shearing rate and the rate sensitivity of slip. The calculation of $\tau_{k,\,\mathrm{crit}}$ has been achieved by accounting for latent hardening through the use of an appropriate hardening matrix,

$$\dot{\tau}_{k,crit} = \sum_i h^{ki} \left|\dot{\gamma}^i\right|, \quad h^{ki} = q^{ki} h^{(i)} \tag{13}$$

where h^{ki} is the rate of strain hardening on *k*th slip system due to a shearing on *i*th slip system, q^{ki} is the hardening matrix describing the latent hardening behavior of a crystallite, and $h^{(i)}$ is hardening rate of single slip system *i*. In the present study, 12 slip systems with crystallographic <110> slip directions and {111} slip planes are taken into account for room temperature simulations of plastic deformation of aluminium. The actual finite element calculations were carried out using the finite element software ABAQUS in conjunction with the user defined material subroutine UMAT. Corresponding simulations can also be conducted using the finite element package MARC.

Simulations and Experiments

The present cup drawing simulations were conducted under the assumption that the circular blank being drawn had an initial radius of 100 mm and a thickness of 0.82 mm. The blank was modeled using 432 C3D8 elements and 80 C3D6 elements. The interaction between the blank and the blank holder was assumed as a so called soft contact to impose the appropriate clamping pressure in the thickness direction of the element between blank, die, and blank holder. The simulations shown below used an exponential soft contact function. Different friction properties (μ=0 to 0.2) were checked and the results showed that friction properties had under these contact conditions only little influence on the ear height. This is an important aspect compared to conventional J2-based continuum plasticity simulations which generally reveal stronger dependence on friction. Consequently the μ=0 case was selected to save computing time. It must be noted though that the influence of friction can be significantly different under different boundary conditions (Figs. 3, 4).

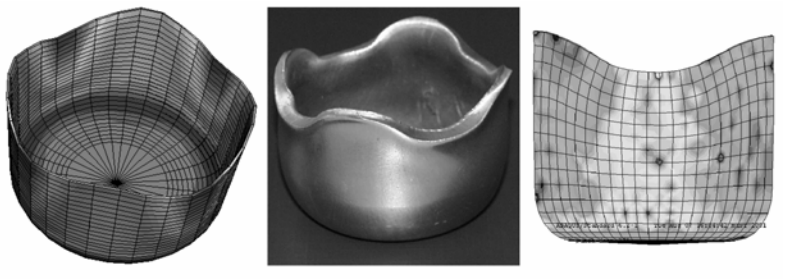

Fig 3 Simulation and experiment of cup drawing, aluminium. Left: The gray scale indicates the sheet thickness. Right: The gray scale indicates the orientation change during drawing.

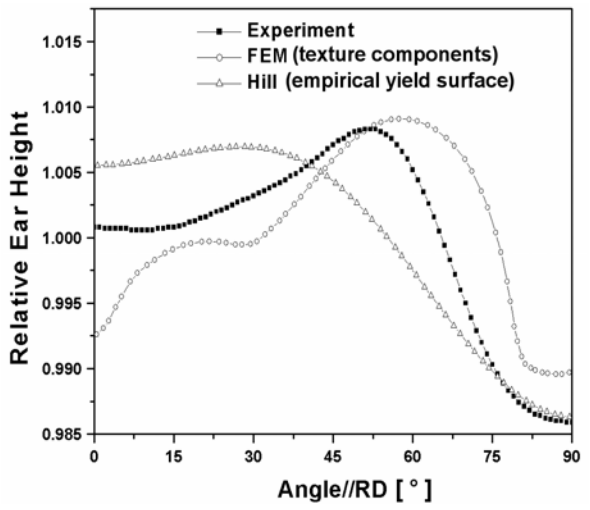

Fig 3 Simulations and experiment of earing for cup drawing, aluminium. Results of the texture component finite element simulation and a simulation obtained by use of a Hill yield surface which was fitted to the texture.

Summary

We discussed a new finite element method which includes and updates texture during forming simulations. The method is based on feeding texture components into a crystal plasticity FE model. We presented a comparison between experiment (aluminium), the new component approach, and a Hill-based yield surface simulation which does not update the texture during loading.

References

[1] Z. Zhao, F. Roters, W. Mao and D. Raabe: Adv. Eng. Mater. Vol. 3 (2001), p. 984

[2] D. Raabe, Z. Zhao and F. Roters: Steel Research Vol. 72 (2001), p. 421

[3] H. J. Bunge: *Texture Analysis in Materials Science* (Butterworths, London, 1982)

[4] K. Lücke, J. Pospiech, K. H. Virnich and J. Jura: Acta Metall. Vol. 29 (1980), p. 167

[5] K. Helming., R.A. Schwarzer, B. Rauschenbach, S. Geier, B. Leiss, H. Wenk, K. Ullemeier and J. Heinitz, Z. Metallkd. Vol. 85 (1994), p. 545

[6] K. Helming: *Texturapproximation durch Modellkomponenten* (in German), (Cuvillier Verlag Göttingen, Germany, 1996)

[7] S. R. Kalidindi, C. A. Bronkhorst and L. Anand, J. Mech. Phys. Solids Vol. 40 (1992), p. 537

Additional Report References

D. Raabe, M. Sachtleber, Z. Zhao, F. Roters, S. Zaefferer: Acta Materialia 49 (2001) 3433–3441

„Micromechanical and macromechanical effects in grain scale polycrystal plasticity experimentation and simulation”

D. Raabe, Z. Zhao, S.–J. Park, F. Roters: Acta Materialia 50 (2002) 421–440

„Theory of orientation gradients in plastically strained crystals”

Z. Zhao, F. Roters, W. Mao, D. Raabe: Adv. Eng. Mater. 3 (2001) p.984/990

„Introduction of A Texture Component Crystal Plasticity Finite Element Method for Industry-Scale Anisotropy Simulations”

D. Raabe, P. Klose, B. Engl, K.-P. Imlau, F. Friedel, F. Roters: Advanced Engineering Materials 4 (2002) 169-180

„Concepts for integrating plastic anisotropy into metal forming simulations”

D. Raabe, Z. Zhao, W. Mao: Acta Materialia 50 (2002) 4379–4394

„On the dependence of in-grain subdivision and deformation texture of aluminium on grain interaction”

D. Raabe: Advanced Engineering Materials 4 No. 5 (2002) p. 255-267

„Don’t Trust your Simulation - Computational Materials Science on its Way to Maturity ?”

D. Raabe: Advanced Materials 14 No. 9 (2002) p. 639-650

„Challenges in Computational Materials Science”

D. Raabe and F. Roters: International Journal of Plasticity 20 (2004) p. 339-361

„Using texture components in crystal plasticity finite element simulations”

D. Raabe, M. Sachtleber, H. Weiland, G. Scheele, and Z. Zhao: Acta Materialia 51 (2003) 1539-1560.

„Grain-scale micromechanics of polycrystal surfaces during plastic straining”

S. Zaefferer, J.-C. Kuo, Z. Zhao, M. Winning, D. Raabe: Acta Materialia 51 (2003) 4719-4735.

„On the influence of the grain boundary misorientation on the plastic deformation of aluminum bicrystals”

J.-C. Kuo, S. Zaefferer, Z. Zhao, M. Winning, D. Raabe: Advanced Engineering Materials, 2003, 5, (No.8) 563-566

„Deformation Behaviour of Aluminium-Bicrystals”

Z. Zhao, W. Mao, F. Roters, D. Raabe: Acta Materialia 52 (2004) 1003–1012

„A texture optimization study for minimum earing in aluminium by use of a texture component crystal plasticity finite element method”